

pubs.acs.org/JPCB Article

Structural Dynamics and Topology of the Inactive Form of S²¹ Holin in a Lipid Bilayer Using Continuous-Wave Electron Paramagnetic Resonance Spectroscopy

Tanbir Ahammad, Daniel L. Drew, Rasal H. Khan, Indra D. Sahu, Emily Faul, Tianyan Li, and Gary A. Lorigan*



Cite This: J. Phys. Chem. B 2020, 124, 5370-5379



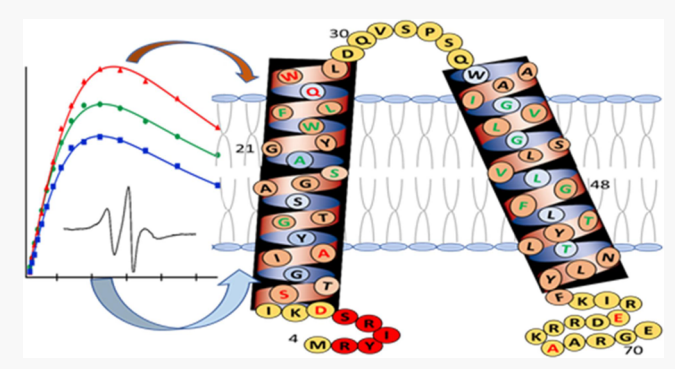
ACCESS

Metrics & More

Article Recommendations

Supporting Information

ABSTRACT: The bacteriophage infection cycle plays a crucial role in recycling the world's biomass. Bacteriophages devise various cell lysis systems to strictly control the length of the infection cycle for an efficient phage life cycle. Phages evolved with lysis protein systems, which can control and fine-tune the length of this infection cycle depending on the host and growing environment. Among these lysis proteins, holin controls the first and rate-limiting step of host cell lysis by permeabilizing the inner membrane at an allele-specific time and concentration hence known as the simplest molecular clock. Pinholin S^{21} is the holin from phage $\Phi 21$, which defines the cell lysis time through a predefined ratio of active pinholin and antipinholin (inactive form of pinholin). Active pinholin and antipinholin fine-tune the lysis



timing through structural dynamics and conformational changes. Previously we reported the structural dynamics and topology of active pinholin S²¹68. Currently, there is no detailed structural study of the antipinholin using biophysical techniques. In this study, the structural dynamics and topology of antipinholin S²¹68_{IRS} in DMPC proteoliposomes is investigated using electron paramagnetic resonance (EPR) spectroscopic techniques. Continuous-wave (CW) EPR line shape analysis experiments of 35 different R1 side chains of S²¹68_{IRS} indicated restricted mobility of the transmembrane domains (TMDs), which were predicted to be inside the lipid bilayer when compared to the N- and C-termini R1 side chains. In addition, the R1 accessibility test performed on 24 residues using the CW-EPR power saturation experiment indicated that TMD1 and TMD2 of S²¹68_{IRS} were incorporated into the lipid bilayer where N- and C-termini were located outside of the lipid bilayer. Based on this study, a tentative model of S²¹68_{IRS} is proposed where both TMDs remain incorporated into the lipid bilayer and N- and C-termini are located outside of the lipid bilayer. This work will pave the way for the further studies of other holins using biophysical techniques and will give structural insights into these biological clocks in molecular detail.

INTRODUCTION

Much of the world's biomass is recycled by the bacteriophage infection cycle, which repeats $\sim 10^{28}$ times per day and must be precisely controlled to maintain the phage's ability to continue this cycle. Bacteriophage-infected Gram-negative bacterial cell lysis is accomplished in a controlled way by at least three groups of phage lysis proteins. These lysis proteins include holin, endolysin, and spanin. They are responsible for the permeabilization of the inner membrane, degradation of the peptidoglycan layer and the outer membrane, respectively.²⁻ The proper timing of infected host cell lysis is crucial for the phage life cycle.⁵ Holin plays significant roles in defining the length of the phage infection cycles. 5,6 Consequently, it is subjected to immense evolutionary pressure to achieve the optimum lysis time. Holins are the gatekeepers of the infected cell lysis process and are regulated by several kinds of protein inhibitors. Most of the holins are coexpressed with an inhibitory holin called antiholin.^{5,7} Although some of the holins maintain their regulatory function without a known antiholin or in the absence of a complementary antiholin, it is well accepted that the precise timing of these simplest biological/molecular clocks is attributed to their corresponding antiholins.⁶ Some groups of holins (e.g., S105, S²¹) were extensively studied with an emphasis on the active forms of holins due to its direct biological significance.^{1,7-14} However, structural, dynamic, and topology studies of antiholins are less

Received: April 22, 2020 Revised: June 3, 2020 Published: June 5, 2020





studied despite their significant difference in structure and topology.

Pinholin S^{21} encoded by the S21 gene of phage Φ 21 is significantly different from canonical holins. It makes very small holes in comparison to the canonical holins and destroys the proton motive force to release and activate the signalanchor release (SAR) endolysin at an allele-specific time and concentration. 1,15 The S21 is a dual start motif gene, which encodes the 71 amino acid long antipinholin ($S^{21}71$) or the 68 amino acid long pinholin (S²¹68), each containing two putative transmembrane domains (TMDs). Both TMDs are incorporated into the inner cytoplasmic membrane, keeping the Nand C-termini in the cytoplasm. However, TMD1 of S2168 externalizes very quickly from the inner membrane, exposing itself to the periplasm. The extra three amino acids in the Nterminal of S²¹71 add an extra positive charge, which delays the externalization of TMD1 from the lipid bilayer. Some studies have indicated that pinholin makes homo/hetero dimers and remains inactive unless both TMD1s of a dimer are externalized from the lipid bilayer to make active dimers. 10 Hence, S²¹71 delays the formation of the active dimer, which is a prerequisite for pinholes formation. 10,12 A proper combination of active pinholin and antipinholin gives the precise timing of host cell lysis.6

Although antipinholin $S^{21}71$ delays the holin triggering time, TMD1 still externalizes after an initial delay and behaves like active pinholin, which makes it difficult to study the structural topology of antipinholin $S^{21}71$. Ry Young's group reported a modified form of antipinholin by adding five extra amino acids (RYIRS) after the methionine-4 (M4) of the active pinholin, referred to as $S^{21}68_{IRS}$. This 'RYIRS' tag prevents the externalization of TMD1 from the lipid bilayer due to the bulky side chains and two extra positive charges. It is reported as a dominant inhibitor of pinholin, which makes it more feasible for the study of the inactive form of pinholin $S^{21}.^{21,12}$ In this study, this inactive analog of pinholin ($S^{21}.^{21,12}$ is used to study the structural dynamics and topology of antipinholin of phage $\Phi 21$.

Most of the studies reported on holin and pinholin were conducted using biomolecular and functional techniques.^{1,/-} However, structural dynamics, conformational changes, and topology of antipinholin have not been extensively studied using a variety of biophysical techniques. It is well recognized that proteins' stability and functions are coined in its structural topology and dynamics relationship. 16-20 As a membrane protein, it is important to know the structure and dynamics of this protein in a lipid environment. The study of membrane proteins in the presence of a lipid environment is very challenging using conventional biophysical techniques such as X-ray crystallography and NMR spectroscopy. 21-24 Electron paramagnetic resonance (EPR) spectroscopy is a powerful biophysical technique used to study the structural dynamics and topology of membrane proteins in lipid environments with higher sensitivity and without any size limitation. 16,25-35

In this study, the structural dynamics and topology of antipinholin ($S^{21}68_{IRS}$) in proteoliposomes were investigated using EPR spectroscopic techniques. The full-length antipinholin ($S^{21}68_{IRS}$) was synthesized using Fmoc solid-phase peptide synthesis (Fmoc-SPPS) for convenient spin labeling and high-yield protein sample preparation. Nitroxide spinlabel, MTSL (S-(1-oxyl-2,2,5,5-tetramethyl-2,5-dihydro-1H-pyrrol-3-yl) methyl ethanesulfonothioate) was attached sitespecifically using site-directed spin labeling (SDSL) to make an

EPR active antipinholin construct.^{36,37} Based on our CW-EPR spectroscopic line shape analysis and EPR power saturation data, a tentative structural topology model of the antipinholin S²¹68_{IRS} is proposed, where both TMD1 and TMD2 remains incorporated into the lipid bilayers while the N-terminal, C-terminal, and loop regions remained solvent-exposed.

■ EXPERIMENTAL METHODS

Peptide Synthesis and Purification. All peptides were synthesized on an automated CEM Liberty Blue peptide synthesizer equipped with a Discovery Bio microwave system via optimized Fmoc solid-phase peptide synthesis (SPPS) reported in previous studies.^{37,38} Each synthesis was started with a glutamate-preloaded TGA resin in a dimethylformamide (DMF) based solvent system. Piperidine (20% (v/v)) in DMF was used as a deprotector to remove the Fmoc-protecting group before each coupling cycle. During each coupling cycle, 0.2 M amino acid was added to the reaction vessel in the presence of 15.6% (v/v) N, N'-diisopropylcarbodiimide (DIC) and 14.2% (w/v) oxyma as an activator and activator base, respectively. After successful synthesis, the cleavage reaction was run for at least 3 h under optimized cocktail conditions followed by filtration, N2 (g) evaporation and ether precipitation. 37-40 Peptide pellets were washed three more times with ice-cool ether followed by centrifugation and the precipitated peptide was lyophilized to get a fluffy and easy to solubilize powder peptide. The crude peptide was purified by reverse-phase high-performance liquid chromatography (RP-HPLC) using a GE HPLC system coupled with a C4 (10 μ m) preparative column (Vydac 214TP, 250 × 22 mm). A two solvent gradient system was used, where the polar solvent was 100% water and the nonpolar solvent was 90% acetonitrile with 10% of water. TFA (0.1%) was added to both the solvents to acidify them.

To attach the spin-label to the peptide, the lyophilized pure peptide was dissolved in dimethyl sulfoxide (DMSO) with a fivefold excess of MTSL (1:5 molar ratio) and stirred for 24 h in a dark environment. The spin-labeled (SL) peptide was lyophilized again and purified with a C4 semipreparative column (Vydac 214TP, 250 \times 10 mm), using the same solvent and gradient system to remove free MTSL and further purify the peptide sample. After each purification, the purity of the target peptide was confirmed by MALDI-TOF MS. Spin-labeling efficiency was calculated to be \sim 85 to 90% using CW-FPR 38

Peptide Incorporation into Proteoliposomes. To mimic the membrane environment spin-labeled antipinholin peptides were incorporated into DMPC (1,2-dimyristoyl-snglycero-3-phosphocholine) proteoliposomes following the thin film method. 37,38 In brief, the pure spin-labeled peptide was dissolved in 2,2,2-trifluoroethanol (TFE) and mixed with predissolved DMPC lipid solution in a pear-shaped flask. The organic solvent was gently evaporated by $N_2(g)$ purging to get a uniformly thin film inside the pear-shaped flask followed by overnight vacuum desiccation to remove any residual organic solvent. A 10 mM HEPES (4-(2-hydroxyethyl)-1-piperazineethan esulfonic acid) buffer (pH \sim 7.0) was used to rehydrate the thin film to get a final concentration of 200 mM lipid and 200 μM peptide within the proteoliposomes sample. Before rehydration, both HEPES buffer and the sample flask were kept in a warm water bath for a short period of time to bring the temperature above the phase transition temperature of DMPC. 37,41,42 The lipid film was dispersed from the flask

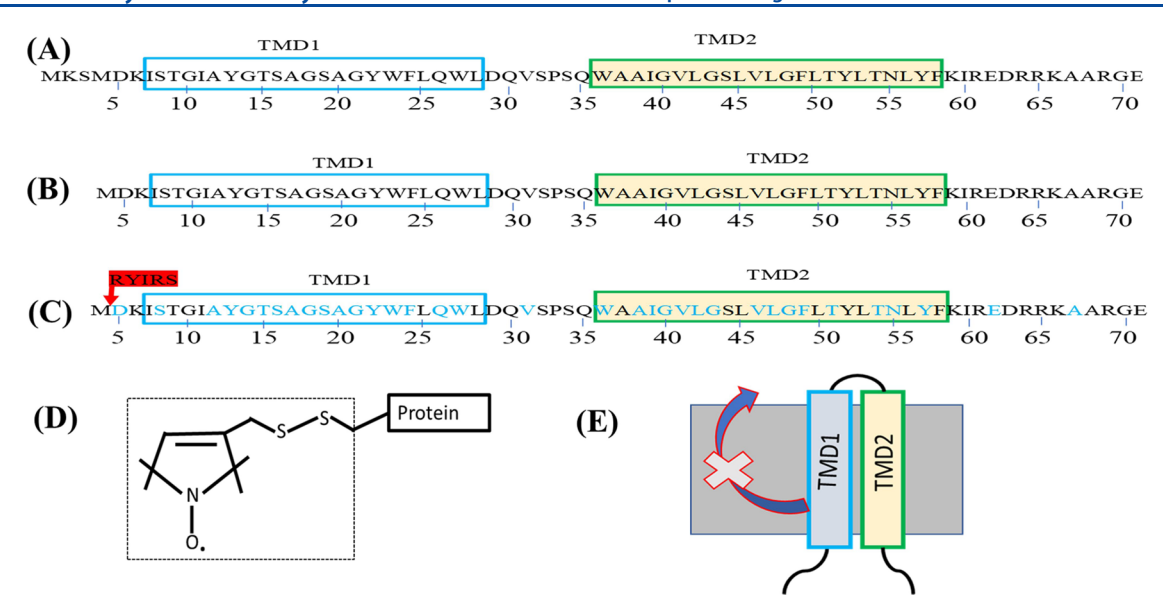


Figure 1. Primary sequences of (A) wild type antipinholin $S^{21}71$, (B) wild type active pinholin $S^{21}68$, and (C) inactive analog of pinholin $S^{21}(S^{21}68_{IRS})$. The amino acid positions studied by EPR spectroscopy are shown in blue. The inactive tag is color-coded red and indicating its incorporation site by the arrow. The helical region of TMD1 and TMD2 are indicated by blue and green boxes, respectively. (D) MTSL attached to Cys side chain of the protein via a disulfide bond (also known as R1). (E) Predicted topology of $S^{21}68_{IRS}$ where both TMDs remain incorporated in the lipid bilayer and TMD1 has not been externalized from the lipid bilayer. 10,12,15,37

sidewall by vortexing several times followed by warming in a hot water bath. At least three freeze—thaw cycles were performed before adding glycerol. Glycerol was added to give a final concentration of 10% and mixed thoroughly, which helped the sample remain suspended for a longer duration at room temperature without phase separation. Sample homogeneity and proteoliposomes size were confirmed by using dynamic light scattering (DLS) spectroscopy (ZETASIZER NANO Series; Malvern Instruments) at 25 °C in a disposable 40 μ L microcuvette.

Circular Dichroism Spectroscopy. Circular Dichroism (CD) data for antipinholin S²¹68_{IRS} were collected using an Aviv Circular Dichroism Spectrometer (Model 435) in a quartz cuvette with a 1.0 mm path length. The pure peptide sample was dissolved in TFE to obtain the CD spectra in the solution form. Data were collected from 260 to 200 nm with an average of three scans per sample and 1 nm bandwidth at 25 °C.

CW-EPR Spectroscopy. CW-EPR spectra were collected at X-band (~9.34 GHz) with a Bruker EMX spectrometer equipped with an ER041xG microwave bridge and an ER4119-HS cavity at the Ohio Advanced EPR Laboratory at Miami University. Each spectrum was acquired by signal-averaging 10 scans with 3315 G central field, sweep width 150 G, 42 s field sweep, 100 kHz modulation frequency, 1 G modulation amplitude, and 10 mW microwave power.³⁷ Each experiment was repeated at least three times at room temperature.

Spin-Label Mobility Analysis. The inverse line width (δ^{-1}) of the first derivative central resonance line $(m_{\rm I}=0)$ was calculated to determine the side chain mobility. To further explore the dynamic properties, the rotational correlation time (τ) was calculated using eq 1: $^{32,33,43-45}$

$$\tau = K \delta \left[\sqrt{\left(\frac{h_0}{h_{-1}} - 1\right)} - 1 \right]$$
(1)

where $K = 6.5 \times 10^{-10}$ s, δ is the width of the central line, and h_0 and h_{-1} are the heights of the center and high field lines, respectively. ^{44,45}

CW-EPR Power Saturation Experiments. CW-EPR power saturation experiments were performed on a Bruker EMX X-band spectrometer coupled with an ER 041XG microwave bridge and an ER 4123D CW-Resonator (Bruker BioSpin). Experimental setups were optimized following published literature articles. 28,34,46 Samples were loaded into gas permeable TPX capillary tubes with a total volume of 3–4 μ L at a concentration of 100–150 μ M. ^{46–49} EPR spectroscopic data were collected using a modulation amplitude of 1.0 G, a modulation frequency of 100 kHz, 42 s field sweep, and 90 G sweep width. Incident microwave powers were varied from 0.06 to 159 mW. At each microwave power, three to five scans were taken for signal-averaging. For each spin-labeled site, the spectra were recorded under three equilibrium conditions and at each condition, experiments were repeated at least three times. At first, the samples were equilibrated with a lipidsoluble paramagnetic relaxant (21% oxygen) followed by equilibration with nitrogen gas (as a control), and equilibration with a water-soluble paramagnetic relaxant (2 mM NiEDDA) with a continuous purge of nitrogen gas. 37,49 NiEDDA was synthesized according to the published protocol. 35,49 The samples were purged with nitrogen gas for at least 1 h, at a rate of 10 mL per minute before starting nitrogen or NiEDDA data acquisition. The resonator was connected to the gas supply (air (as a source of 21% oxygen) or nitrogen gas) during all measurements, and all the experiments were performed at room temperature. The peak-to-peak amplitudes (A) of the first derivative $m_1 = 0$ resonance lines were extracted and plotted against the square root of the incident microwave power. These data points were then fitted according to eq

$$A = I\sqrt{P} \left[1 + \frac{(2^{1/\varepsilon} - 1)P}{P_{1/2}} \right]^{-\varepsilon}$$
 (2)

where I is a scaling factor, $P_{1/2}$ is the power where the first derivative amplitude is reduced to half of its unsaturated value, and ε is a measure of the homogeneity of saturation of the resonance line. For the homogeneous and inhomogeneous saturation limits, $\varepsilon=1.5$ and $\varepsilon=0.5$, respectively. In eq 2, I, ε , and $P_{1/2}$ are adjustable parameters and yield a characteristic $P_{1/2}$ value for each equilibrium condition. Data analysis was performed using a MATLAB software script. The corresponding depth parameter (Φ) was calculated using eq 3:³⁵

$$\Phi = \ln \left[\frac{\Delta P_{1/2}(O_2)}{\Delta P_{1/2}(NiEDDA)} \right]$$
(3)

where $\Delta P_{1/2}(\mathrm{O_2})$ is the difference in the $P_{1/2}$ values for oxygen and nitrogen equilibriums, and $\Delta P_{1/2}(\mathrm{NiEDDA})$ is the difference in the $P_{1/2}$ values for NiEDDA and nitrogen equilibriums.

RESULTS

Recently, the structural topology and dynamic properties of active pinholin S2168 was reported using CW-EPR spectroscopic techniques.³⁷ In this study, the structural dynamics and topology of the antipinholin S²¹68_{IRS} peptide incorporated into DMPC proteoliposomes were investigated using CW-EPR spectral line shape analysis and power saturation experiments. The spin-labeled positions were judiciously selected based on the published literature and initial experimental data to minimize structural perturbations. 10 Figure 1A,B shows the primary sequence of the S²¹71and S²¹68, which are wild type antipinholin and active pinholin, respectively, as a quick reference and comparison with the reporting antipinholin allele. Figure 1C shows the primary sequence of the inactive analog of pinholin S^{21} ($S^{21}68_{IRS}$) where the spin-label positions are indicated in blue. MTSL was attached to the Cys side chain where Cys replaced the native amino acid in the site-specific position. MTSL attached to Cys side chain, known as R1 is shown in Figure 1D. The predicted topology of $S^{21}68_{IRS}$ is adapted from the literature and shown in Figure 1E. 1,10,12,38,50

Pure spin-labeled peptide samples were obtained by double purification using RP-HPLC and confirmed by MALDI-TOF MS. A representative HPLC and MS spectra are shown in Supporting Information (SI) Figure S1. Proteoliposome sample size and homogeneity were investigated using DLS. A representative DLS spectrum is shown in Figure 2. It shows homogenous proteoliposomes with a maximum intensity of around 124 nm.

Proper folding and alpha-helical secondary structure of the peptide samples were examined by CD measurements. CD spectra were obtained for the antipinholin $S^{21}68_{IRS}$ with and without spin-label in TFE solution to confirm that the spin-label incorporation has no significant effects on the secondary structure. Figure 3 shows representative CD spectra for antipinholin $S^{21}68_{IRS}$ without spin-label (black solid line) and antipinholin $S^{21}68_{IRS}$ F24R1, spin-labeled at the F24 position (blue solid line). In Figure 3, both spectra exhibit two minima at 222 and 208 nm, which suggest that both samples have α -helical secondary structures in the TFE solution. These CD data confirmed that nitroxide spin-labeling has no significant effect on the global secondary structure.

Structural Dynamics of Antipinholin S²¹68_{IRS}. CW-EPR spectral analysis is a powerful biophysical technique used to decipher the structural dynamics properties of a protein at a residue-specific level with spatial resolution. ^{43,52–56} To probe

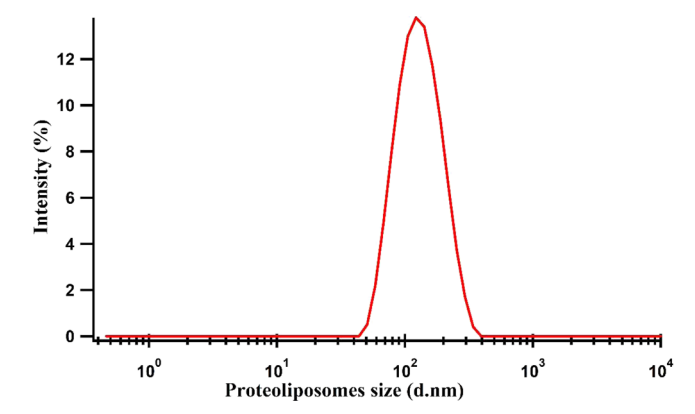


Figure 2. DLS spectrum for $S^{21}68_{IRS}$ F49R1 incorporated into the DMPC proteoliposomes. Signal intensity is plotted as a log function of the particle diameter.

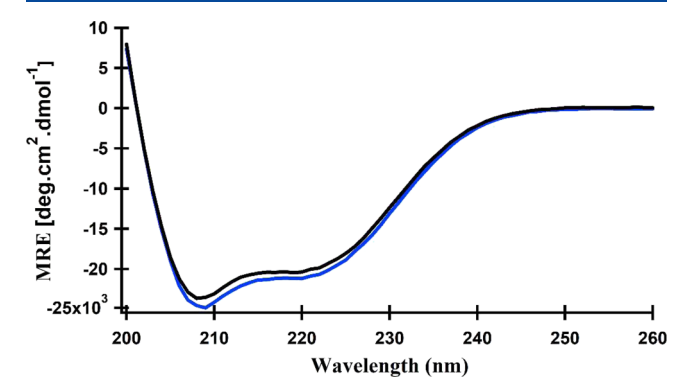


Figure 3. (A) Circular dichroism spectra for inactive pinholin $S^{21}68_{IRS}$ without spin-label (black) and $S^{21}68_{IRS}$ F24R1, with spin-label (blue). Spectra were signal-averaged for three scans. Mean residue molar ellipticity (MRE) is plotted against the incident radiation wavelength.

the structural dynamics of $S^{21}68_{IRS}$, a total of 35 CW-EPR spectra of the R1 side chain were analyzed, which were placed at strategic locations of $S^{21}68_{IRS}$, as shown in Figure 1C. Figure 4 shows representative CW-EPR spectra collected for R1 side chains placed at the N-terminal, TMD1, TMD2, and C-terminal regions of $S^{21}68_{IRS}$ in DMPC proteoliposomes.

All CW-EPR spectra show the conventional three peaks of the nitroxide spin-label due to the ¹⁴N hyperfine splitting. Higher mobility of the R1 side chain in the terminal regions was confirmed by the sharper peaks. TMD-located R1 spectra, indicated restricted mobility by virtue of the broader central peak. Most of the EPR spectra showed a single motional component. However, some spectra (e.g., W23R1, G40R1, G48R1, T51R1, N55R1, and Y57R1) showed two spectral components (rigid/slower and fast/higher motional components), which are indicative of heterogeneous dynamics of the R1 spin label.⁵² CW-EPR spectra with a significant population of rigid components (W23R1, N55R1, and Y57R1) are indicated by (*) in Figure 4. Different motional components can be observed on the R1 spectra when the motion of the spin label is restricted by a heterogeneous interaction with the local environment. 57 These residues are close to the end of TMD1/ TMD2 and near the lipid/solvent interface, which could induce heterogeneous interaction.⁵³ Another reason may be the presence of the bulky side chains on the same side of the helix.⁵⁷ Here, Q26 and W27 have bulky side chains, which are present on the same side of W23 and may cause multiple

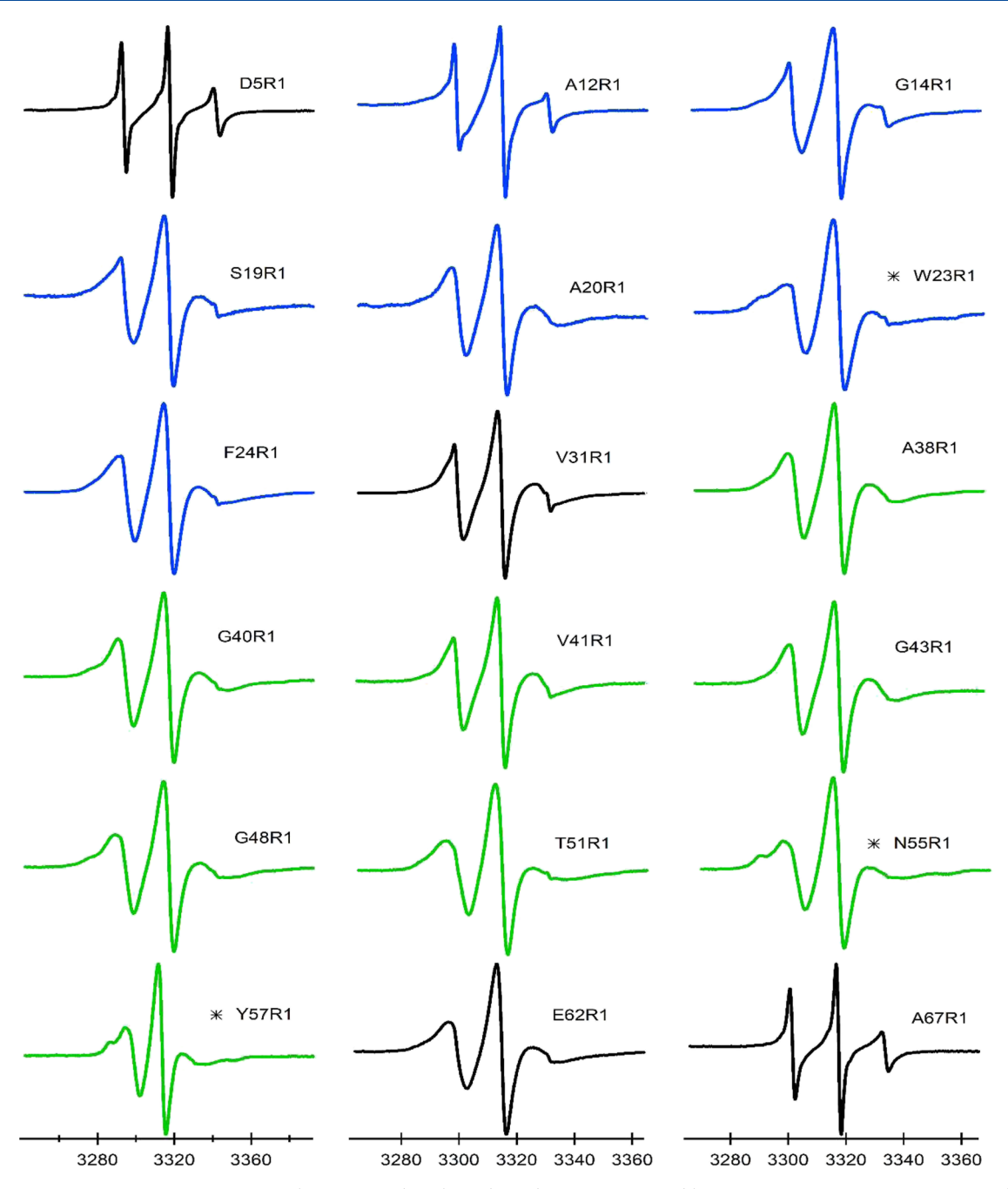


Figure 4. Representative CW-EPR spectra with R1 situated at the indicated positions. Here, blue EPR spectra represent TMD1 residues, green represents TMD2, and black indicates loop and terminal regions. All spectra were normalized to the highest spectral intensity. CW-EPR spectra composed of multiple components were marked with (*).

motional components for the W23R1 spectrum. Similarly, Y52 with the bulky side chain present on the same side of N55 causes multiple motional components for N55R1.

To quantify the dynamic properties of antipinholin $S^{21}68_{IRS}$, the width of the central resonance line (δ) was measured and the inverse of the width of the central resonance line (δ^{-1}) was calculated. Inverse width of the central resonance line (δ^{-1}) is known as the relative mobility of the spin label and has been used as a semiquantitative measurement of nitroxide mobility. The mobility of individual residues is shown in Figure 5, by plotting δ^{-1} as a function of residue positions for pinholin $S^{21}68_{IRS}$.

Both TMDs had restricted mobility when compared to the N- and C-termini residues, which imply that TMDs are incorporated into the lipid bilayer where N- and C-termini residues are solvent-exposed and had less interaction with the surrounding environments. The highest mobility was observed for S8R1 (0.62 G⁻¹), present in the N-terminal, while the lowest mobility was observed for T51R1(0.22 G⁻¹), present in the TMD2. A greater range of values for δ^{-1} are observed for TMD1, when compared to that observed in TMD2, specifically in the N-terminal side of TMD1. The N-terminal of TMD1 (first 3 \sim 4 amino acids) had significantly higher mobility in comparison with the rest of the helical region implying that

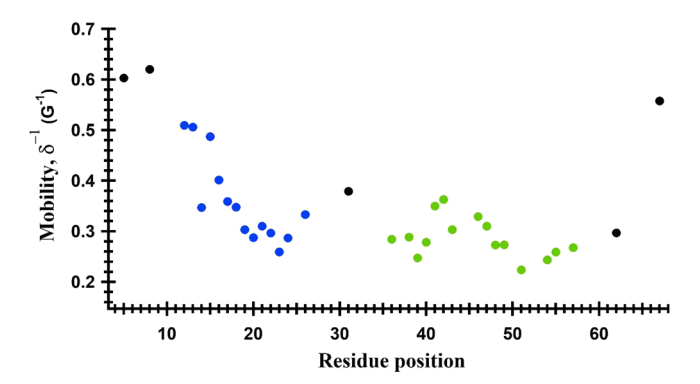


Figure 5. Relative mobility of R1 (δ^{-1}) as a function of residue positions of the primary sequence of $S^{21}68_{IRS}$. A higher value of (δ^{-1}) indicates the higher mobility of the nitroxide spin-label at that corresponding position. Here, blue closed circles represent TMD1 residues, green represents TMD2, and black indicates loop and terminal regions.

this segment was outside of the lipid bilayer and had less interaction with surrounding environments.

To further quantify the relative motion of different side chains of $S^{21}68_{IRS}$, the rotational correlational time (τ) was calculated for the nitroxide spin-label placed in corresponding positions of $S^{21}68_{IRS}$. The rotational correlational time (τ) is the time required for the spin-label to rotate 1 radian and calculated by using the empirical formula shown in eq $1.^{43}$ The calculated τ values are indicative of backbone fluctuations, side chain dynamics, and interactions of the side chain with the surroundings. 37,59,60 Figure 6 represents the calculated τ values for the corresponding residues of spin-labeled inactive pinholin $S^{21}68_{IRS}$.

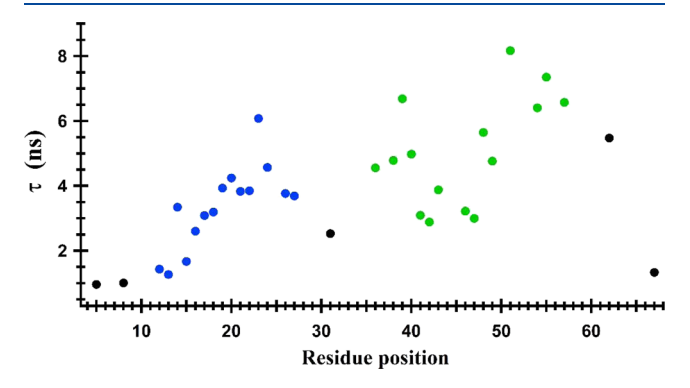


Figure 6. Rotational correlational time (τ) as a function of residue positions of the primary sequence of $S^{21}68_{IRS}$. The same color code is used as in Figure 5.

Shorter τ values for N- and C-termini residues suggest higher spin-label motion and imply that these segments were outside of the lipid bilayer. Conversely, longer τ for TMDs residues suggest their restricted motion due to the lipid environment and/or restricted backbone motions. The minimum and maximum τ values were calculated to be 1.0 ns (D5R1 and S8R1) and 8.2 ns (T51R1), respectively. Dynamic patterns observed from the τ value calculation are consistent with the side chain mobility data extracted from the central line broadening shown in Figure 5.

Structural Topology and Interaction of $S^{21}68_{IRS}$ with the Lipid Bilayer. To explore the interaction and incorporation of antipinholin $S^{21}68_{IRS}$ into DMPC proteolipo-

somes, CW-EPR power saturation experiments were carried out in the presence of lipid-soluble (oxygen) and water-soluble (NiEDDA) paramagnetic relaxants. Oxygen and NiEDDA primarily probe the relative abundance and accessibility of the nitroxide spin-label in the lipid and aqueous phase, respectively. 61 Relative accessibility of the particular spin label to the lipid-soluble and water-soluble paramagnetic relaxing agents provides information on whether this spin label is within the lipid environment or exposed to the aqueous environment. Figure 7 represents CW-EPR power saturation curves showing the relative signal intensity and saturation pattern as a function of square root of the microwave power for S²¹68_{IRS} A20R1 (Figure 7A) and A67R1(Figure 7B) spin-label positions. S²¹68_{IRS} A20R1 required higher microwave power to reach the saturation in the presence of oxygen when compared to that in the presence of nitrogen and NiEDDA, which qualitatively indicates that this position of spin-label was incorporated into the lipid bilayer and was more accessible to oxygen and less accessible to NiEDDA. Conversely, S²¹68_{IRS} A67R1 was more accessible to NiEDDA than oxygen, indicating that this position was outside of the lipid bilayer.

A total of 24 spin-labeled S²¹68_{IRS} positions were studied via the CW-EPR power saturation technique. The positions are color-coded in the primary sequence of antipinholin (S²¹68_{IRS}) where red are the positions found outside of the lipid bilayer and green are the positions found inside the lipid bilayer. CW-EPR power saturation data clearly demonstrate that N-terminal, C-terminal, and loop regions were solvent-exposed and outside of the lipid bilayer where most of the parts of TMD1 and TMD2 were inside of the lipid bilayer.

To predict the relative orientation of TMD1 and TMD2 with respect to the lipid bilayer, the depth parameter (Φ) for individual residues was calculated using eq 3. The depth parameter (Φ) gives a quantitative analysis of the insertion of spin label into the lipid bilayer, which is derived from relative biomolecular collision rates with the molecular oxygen and NiEDDA. The positive (Φ) value is proportional to the membrane insertion whereas the negative (Φ) value is proportional to solvent accessibility. Figure 8 shows the depth parameter (Φ) as a function of the spin-label position for S²¹68_{IRS}.

Negative (Φ) values for the terminal regions confirm that Nand C-termini were solvent-exposed and outside of the lipid bilayer. All the spin-label positions in TMD2 showed positive (Φ) values confirming that the membrane insertion of TMD2 is consistent with the previously proposed model. 12 Close observation of the selected region of TMD2 shown in SI Figure S2 revealed a characteristic pattern (inverted 'V') of membrane-embedded segments of a protein.⁵³ The positive (Φ) values of TMD2 gradually increased from a smaller value to the maximum around the center of the lipid bilayer followed by gradual decrease to the minimum at the end of the lipid bilayer. The highest depth parameter was observed for G48R1 of TMD2 with a Φ value of 1.15, suggesting that this site was close to the central position in the lipid bilayer. A similar trend was observed for TMD1, although there were less data points when compared to TMD2. The highest depth parameter was 1.0 for A20R1 of TMD1. However, some other residues located at the N-terminal side (A12) or C-terminal side (Q26, W27) of the TMD1 showed negative (Φ) values, which imply that starting and ending regions of the helix remain outside of the lipid bilayer. This behavior agrees with the previously proposed topology from the Ry Young Lab. 10,12

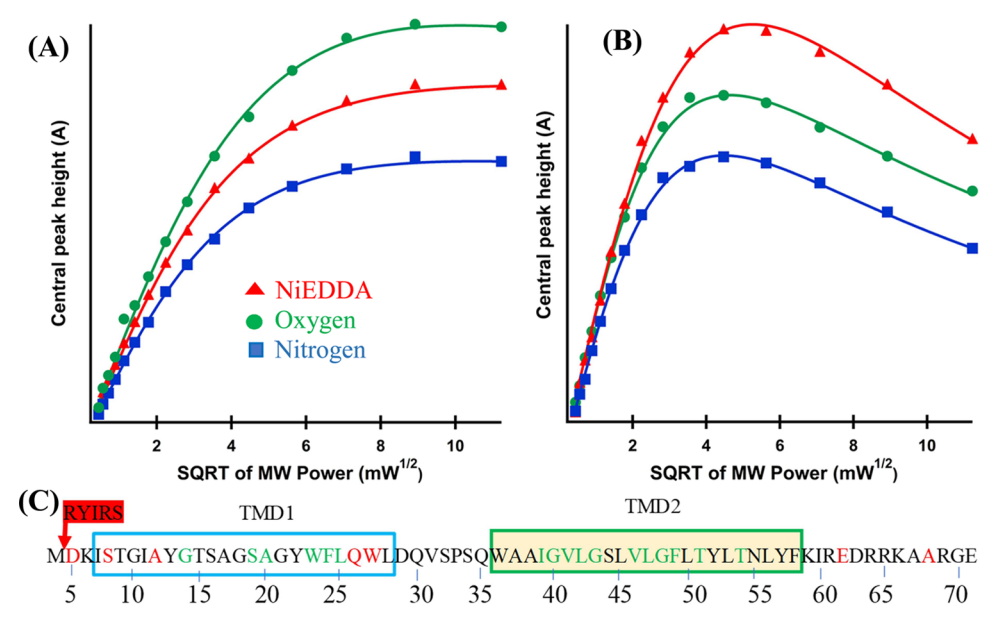


Figure 7. Representative CW-EPR power saturation curves of $S^{21}68_{IRS}$ in DMPC proteoliposomes. (A) A20R1 and (B) A67R1. The red triangle represents NiEDDA, green circle represents oxygen, and blue square represents nitrogen spectra with their fitted line from eq 2. The amplitudes of the first derivative $m_{\rm I}=0$ peak were plotted against the square root (SQRT) of the incident microwave (MW) power. (C) Color-coded primary sequence of $S^{21}68_{IRS}$, where green residues are buried in the lipid bilayer and red residues are solvent-exposed based on the CW-EPR power saturation data.

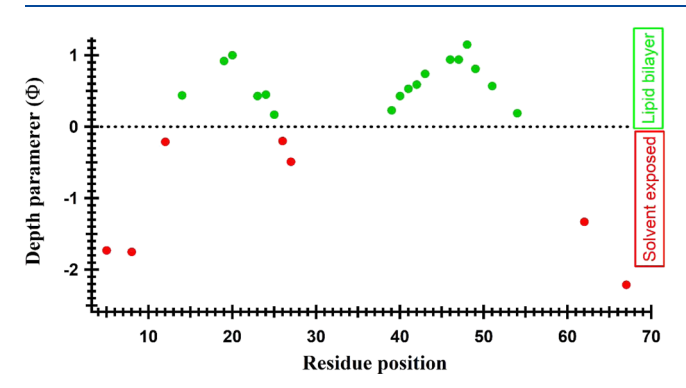


Figure 8. Calculated depth parameter (Φ) as a function of $S^{21}68_{IRS}$ residue positions in DMPC proteoliposomes. Positive (Φ) values (green) indicate that the R1 side chains are embedded inside the lipid bilayer and negative (Φ) values (red) indicate that the R1 side chains are solvent-exposed.

DISCUSSION

This is the first biophysical study of the inactive form of pinholin S²¹ using EPR spectroscopy and illustrated the relative difference in the dynamics of different segments and residues of S²¹68_{IRS}. Terminal regions have significantly higher mobility due to its structural flexibility and a lipid-free environment. Conversely, both TMD regions have restricted mobility, especially the residues, which are predicted to be incorporated into the lipid bilayer. CW-EPR power saturation data were consistent with the mobility data derived from CW-EPR line shape analysis and confirmed the membrane insertion of TMD1 and TMD2 where the N- and C-termini and both ends of the helices were solvent-exposed.

For this EPR spectroscopic study of S²¹68_{IRS}, the spinlabeled positions were judiciously selected based on the published literature and initial experimental data to minimize structural perturbations.¹⁰ This selective spin labeling led to fewer data points for TMD1 when compared with TMD2. Moreover, TMD1 is prone to mutational effects and has a natural tendency to externalize from the lipid bilayer. Some spin-labeled residues of TMD1 were found outside of the membrane, which were expected to be inside of the lipid bilayer (e.g., A17R1 and G21R1). This may be due to the change of hydrophobicity or interruption of the TMD1–TMD2 interaction or both when the native amino acids were replaced with the R1 side chain. These residues were excluded from the topological analysis of antipinholin due to their structural perturbations. It is worthy to mention here that the previous study reported by the Young lab found activation of antipinholin S²¹68_{IRS} when they performed the mutations at some of these positions e.g., S²¹68_{IRS} A17Q, G21Q. On the second structure of the second structure of the second structure of these positions e.g., S²¹68_{IRS} A17Q, G21Q.

Based on the dynamic information and accessibility data reported in this study, a tentative structural topology model of S²¹68_{IRS} is proposed as shown in Figure 9. As shown in Figure 9, residues are color-coded based on power saturation data where red is solvent-exposed, green is located inside of the lipid bilayer, and black is not studied by power saturation. The "RYIRS" tag is indicated by red filled circles. Several residues are labeled with residue positions as a visualization guide. The helical tilt of TMD2 is proposed based on a computational study previously reported by the Young lab and the possible positive hydrophobic mismatch for TMD2. 12,62 Further structural studies are needed to confirm the proposed topology of S²¹68_{IRS}, such as application of double electron—electron resonance (DEER) experiments, which could be performed to refine the structure and relative orientation of TMD1 and TMD2 in the presence of a lipid bilayer.

CONCLUSIONS

This study reported the structural dynamics and topology of the inactive analog of pinholin S^{21} ($S^{21}68_{IRS}$) incorporated into a DMPC lipid bilayer using EPR spectroscopic techniques. Before EPR experiments, the purity and spin-labeling efficiency of all peptide samples were confirmed. It was confirmed that

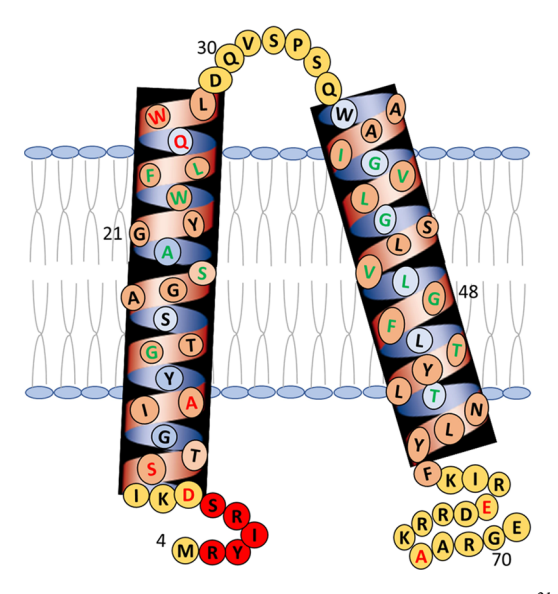


Figure 9. Proposed structural topology of inactive pinholin $S^{21}68_{IRS}$ incorporated into a lipid bilayer. The red amino acids represent solvent-exposed and the green amino acids represent the lipid buried residues based on the CW-EPR power saturation data. Black letters were not studied by the EPR power saturation experiment. Red filled circles are the RYIRS tag used for the inactive conformation of pinholin S^{21} .

protein samples maintained their native secondary structure in all experimental conditions using CD spectroscopy. Spin-label positions were selected judiciously to minimize structural perturbation, while gaining maximum information of structural dynamics and topology of the antipinholin S.²¹ The R1 scanning of antipinholin S²¹68_{IRS} suggested that the N- and C-termini have higher mobility when compared to the two TMDs. The EPR power saturation data indicate that both TMD1 and TMD2 remain in the lipid bilayer. The structural topology model of S²¹68_{IRS} presented in this study will be useful for future structural studies of antipinholin and other holin systems using EPR spectroscopic techniques. Further experiments are recommended to confirm the proposed topology of S²¹68_{IRS}.

ASSOCIATED CONTENT

Supporting Information

The Supporting Information is available free of charge at https://pubs.acs.org/doi/10.1021/acs.jpcb.0c03575.

Representative HPLC and MS spectra (PDF)

AUTHOR INFORMATION

Corresponding Author

Gary A. Lorigan — Department of Chemistry and Biochemistry, Miami University, Oxford, Ohio 45056, United States;
orcid.org/0000-0002-2395-3459; Phone: (513) 529-2813; Email: gary.lorigan@miamioh.edu; Fax: (513) 529-5715

Authors

Tanbir Ahammad – Department of Chemistry and Biochemistry, Miami University, Oxford, Ohio 45056, United States

Daniel L. Drew – Department of Chemistry and Biochemistry, Miami University, Oxford, Ohio 45056, United States Rasal H. Khan – Department of Chemistry and Biochemistry, Miami University, Oxford, Ohio 45056, United States

Indra D. Sahu – Department of Chemistry and Biochemistry, Miami University, Oxford, Ohio 45056, United States; Natural Science Division, Campbellsville University, Campbellsville, Kentucky 42718, United States

Emily Faul – Department of Chemistry and Biochemistry, Miami University, Oxford, Ohio 45056, United States

Tianyan Li – Department of Chemistry and Biochemistry, Miami University, Oxford, Ohio 45056, United States

Complete contact information is available at: https://pubs.acs.org/10.1021/acs.jpcb.0c03575

Notes

The authors declare no competing financial interest.

ACKNOWLEDGMENTS

We are grateful to the members of the Ry Young group at Texas A&M University for their experimental suggestions. We would like to thank Dr. Robert McCarrick for his continuous support for EPR instruments and data analysis. This work was generously supported by the NSF CHE-1807131 grant, the NSF (MRI-1725502) grant, the Ohio Board of Regents, and Miami University. Gary A. Lorigan would also like to acknowledge support from the John W. Steube Professorship.

REFERENCES

- (1) Park, T.; Struck, D. K.; Deaton, J. F.; Young, R. Topological dynamics of holins in programmed bacterial lysis. *Proc. Natl. Acad. Sci. U. S. A.* **2006**, *103*, 19713–19718.
- (2) Young, R. Phage Lysis: Three steps, three choices, one outcome. *J. Microbiol.* **2014**, *52*, 243–258.
- (3) Berry, J.; Rajaure, M.; Pang, T.; Young, R. The spanin complex is essential for lambda lysis. *J. Bacteriol.* **2012**, *194*, 5667–5674.
- (4) Berry, J.; Summer, E. J.; Struck, D. K.; Young, R. The final step in the phage infection cycle: the Rz and Rz1 lysis proteins link the inner and outer membranes. *Mol. Microbiol.* **2008**, *70*, 341–351.
- (5) Young, R. Bacteriophage holins: Deadly diversity. J. Mol. Microbiol. Biotechnol. 2002, 4, 21–36.
- (6) Wang, I. N.; Smith, D. L.; Young, R. Holins: The protein clocks of bacteriophage infections. *Annu. Rev. Microbiol.* **2000**, *54*, 799–825.
- (7) White, R.; Chiba, S.; Pang, T.; Dewey, J. S.; Savva, C. G.; Holzenburg, A.; Pogliano, K.; Young, R. Holin triggering in real time. *Proc. Natl. Acad. Sci. U. S. A.* **2011**, *108*, 798–803.
- (8) Dewey, J. S.; Savva, C. G.; White, R. L.; Vitha, S.; Holzenburg, A.; Young, R. Micron-scale holes terminate the phage infection cycle. *Proc. Natl. Acad. Sci. U. S. A.* **2010**, *107*, 2219–2223.
- (9) Pang, T.; Park, T.; Young, R. Mapping the pinhole formation pathway of S21. Mol. Microbiol. 2010, 78, 710-719.
- (10) Pang, T.; Park, T.; Young, R. Mutational analysis of the S21 pinholin. *Mol. Microbiol.* **2010**, *76*, 68–77.
- (11) White, R.; Tran, T. A. T.; Dankenbring, C. A.; Deaton, J.; Young, R. The N-Terminal Transmembrane Domain of λ S Is Required for Holin but Not Antiholin Function. *J. Bacteriol.* **2010**, 192, 725–733.
- (12) Pang, T.; Savva, C. G.; Fleming, K. G.; Struck, D. K.; Young, R. Structure of the lethal phage pinhole. *Proc. Natl. Acad. Sci. U. S. A.* **2009**, *106*, 18966–18971.
- (13) Moussa, S. H.; Lawler, J. L.; Young, R. Genetic Dissection of T4 Lysis. J. Bacteriol. 2014, 196, 2201–2209.
- (14) Gründling, A.; Bläsi, U.; Young, R. Genetic and Biochemical Analysis of Dimer and Oligomer Interactions of the λ S Holin. *J. Bacteriol.* **2000**, 182, 6082–6090.
- (15) Park, T.; Struck, D. K.; Dankenbring, C. A.; Young, R. The pinholin of lambdoid phage 21: Control of lysis by membrane depolarization. *J. Bacteriol.* **2007**, *189*, 9135–9139.

- (16) Columbus, L.; Hubbell, W. L. A new spin on protein dynamics. *Trends Biochem. Sci.* **2002**, *27*, 288–295.
- (17) Volkman, B. F.; Lipson, D.; Wemmer, D. E.; Kern, D. Two-state allosteric behavior in a single-domain signaling protein. *Science* **2001**, 291, 2429–2433.
- (18) Mulder, F. A. A.; Mittermaier, A.; Hon, B.; Dahlquist, F. W.; Kay, L. E. Studying excited states of proteins by NMR spectroscopy. *Nat. Struct. Biol.* **2001**, *8*, 932–935.
- (19) Rozovsky, S.; Jogl, G.; Tong, L.; McDermott, A. E. Solution-state NMR investigations of triosephosphate isomerase active site loop motion: Ligand release in relation to active site loop dynamics. *J. Mol. Biol.* **2001**, *310*, 271–280.
- (20) Ishima, R.; Freedberg, D. I.; Wang, Y. X.; Louis, J. M.; Torchia, D. A. Flap opening and dimer-interface flexibility in the free and inhibitor-bound HIV protease, and their implications for function. *Structure* **1999**, *7*, 1047–1S12.
- (21) Torres, J.; Stevens, T. J.; Samsó, M. Membrane proteins: the 'Wild West' of structural biology. *Trends Biochem. Sci.* **2003**, 28, 137–144.
- (22) Wüthrich, K. NMR studies of structure and function of biological macromolecules (Nobel Lecture). *J. Biomol. NMR* **2003**, 27, 13–39.
- (23) Schiemann, O.; Prisner, T. F. Long-range distance determinations in biomacromolecules by EPR spectroscopy. *Q. Rev. Biophys.* **2007**, *40*, 1–53.
- (24) Acharya, K. R.; Lloyd, M. D. The advantages and limitations of protein crystal structures. *Trends Pharmacol. Sci.* **2005**, *26*, 10–14.
- (25) Sahu, I. D.; McCarrick, R. M.; Lorigan, G. A. Use of electron paramagnetic resonance to solve biochemical problems. *Biochemistry* **2013**, *52*, *5967*–*5984*.
- (26) Altenbach, C.; Froncisz, W.; Hemker, R.; McHaourab, H.; Hubbell, W. L. Accessibility of nitroxide side chains: Absolute Heisenberg exchange rates from power saturation EPR. *Biophys. J.* **2005**, *89*, 2103–2112.
- (27) Pyka, J.; Ilnicki, J.; Altenbach, C.; Hubbell, W. L.; Froncisz, W. Accessibility and dynamics of nitroxide side chains in T4 lysozyme measured by saturation recovery EPR. *Biophys. J.* **2005**, *89*, 2059–2068
- (28) Hubbell, W. L.; Altenbach, C. investigation of structure and dynamics in membrane-proteins using site-directed spin labeling. *Curr. Opin. Struct. Biol.* **1994**, *4*, 566–573.
- (29) Hubbell, W. L.; McHaourab, H. S.; Altenbach, C.; Lietzow, M. A. Watching proteins move using site-directed spin labeling. *Structure* **1996**, *4*, 779–783.
- (30) Hubbell, W. L.; Gross, A.; Langen, R.; Lietzow, M. A. Recent advances in site-directed spin labeling of proteins. *Curr. Opin. Struct. Biol.* **1998**, *8*, 649–656.
- (31) Hubbell, W. L.; Cafiso, D. S.; Altenbach, C. Identifying conformational changes with site-directed spin labeling. *Nat. Struct. Biol.* **2000**, *7*, 735–739.
- (32) Bates, I. R.; Boggs, J. M.; Feix, J. B.; Harauz, G. Membrane-anchoring and charge effects in the interaction of myelin basic protein with lipid bilayers studied by site-directed spin labeling. *J. Biol. Chem.* **2003**, 278, 29041–29047.
- (33) Klug, C. S.; Feix, J. B. Methods and applications of site-directed spin Labeling EPR Spectroscopy. *Methods Cell Biol.* **2008**, *84*, 617–658.
- (34) Altenbach, C.; Marti, T.; Khorana, H.; Hubbell, W. transmembrane protein-structure spin labeling of bacteriorhodopsin mutants. *Science* **1990**, *248*, 1088–1092.
- (35) Altenbach, C.; Greenhalgh, D. A.; Khorana, H. G.; Hubbell, W. L. A collision gradient-method to determine the immersion depth of nitroxides in lipid bilayers application to spin-labeled mutants of bacteriorhodopsin. *Proc. Natl. Acad. Sci. U. S. A.* 1994, 91, 1667–1671.
- (36) Sahu, I. D.; Lorigan, G. A. Site-directed spin labeling EPR for studying membrane proteins. *Biomed. Res. Int.* **2018**, *2018*, 1.
- (37) Ahammad, T.; Drew, D. L., Jr.; Sahu, I. D.; Serafin, R. A.; Clowes, K. R.; Lorigan, G. A. Continuous Wave Electron Para-

- magnetic Resonance Spectroscopy Reveals the Structural Topology and Dynamic Properties of Active Pinholin S2168 in a Lipid Bilayer. *J. Phys. Chem. B* **2019**, *123*, 8048–8056.
- (38) Drew, D. L., Jr.; Ahammad, T.; Serafin, R. A.; Butcher, B. J.; Clowes, K. R.; Drake, Z.; Sahu, I. D.; McCarrick, R. M.; Lorigan, G. A. Solid phase synthesis and spectroscopic characterization of the active and inactive forms of bacteriophage S21 pinholin protein. *Anal. Biochem.* **2019**, *567*, 14–20.
- (39) Bottorf, L.; Sahu, I. D.; McCarrick, R. M.; Lorigan, G. A. Utilization of 13C-labeled amino acids to probe the α -helical local secondary structure of a membrane peptide using electron spin echo envelope modulation (ESEEM) spectroscopy. *Biochim. Biophys. Acta Biomembr.* **2018**, *1860*, 1447–1451.
- (40) Mayo, D. J.; Sahu, I. D.; Lorigan, G. A. Assessing topology and surface orientation of an antimicrobial peptide magainin 2 using mechanically aligned bilayers and electron paramagnetic resonance spectroscopy. *Chem. Phys. Lipids* **2018**, *213*, 124–130.
- (41) Needham, D.; McIntosh, T. J.; Evans, E. Thermomechanical and transition properties of dimyristoylphosphatidylcholine cholesterol bilayers. *Biochemistry* **2002**, *27*, 4668–4673.
- (42) Marsh, D. Thermodynamics of Phospholipid Self-Assembly. *Biophys. J.* **2012**, *102*, 1079–1087.
- (43) Sahu, I. D.; Craig, A. F.; Dunagan, M. M.; Troxel, K. R.; Zhang, R.; Meiberg, A. G.; Harmon, C. N.; McCarrick, R. M.; Kroncke, B. M.; Sanders, C. R.; et al. Probing structural dynamics and topology of the kcne1 membrane protein in lipid bilayers via site-directed spin labeling and electron paramagnetic resonance spectroscopy. *Biochemistry* **2015**, *54*, 6402–6412.
- (44) Boggs, J. M.; Moscarello, M. A. Effect of basic protein from human central nervous-system myelin on lipid bilayer structure. *J. Membr. Biol.* **1978**, *39*, 75–96.
- (45) Eletr, S.; Keith, A. D. Spin-label studies of dynamics of lipid alkyl chains in biological-membranes role of unsaturated sites. *Proc. Natl. Acad. Sci. U. S. A.* **1972**, *69*, 1353–1357.
- (46) Yu, L.; Wang, W.; Ling, S.; Liu, S.; Xiao, L.; Xin, Y.; Lai, C.; Xiong, Y.; Zhang, L.; Tian, C. CW-EPR studies revealed different motional properties and oligomeric states of the integrin β 1a transmembrane domain in detergent micelles or liposomes. *Sci. Rep.* **2015**, *5*, 7848.
- (47) Popp, C. A.; Hyde, J. S. Effects of oxygen on EPR spectra of nitroxide spin-label probes of model membranes. *J. Magn. Reson.* **1981**, 43, 249–258.
- (48) Klug, C. S.; Su, W.; Feix, J. B. Mapping of the Residues Involved in a Proposed β -Strand Located in the Ferric Enterobactin Receptor FepA Using Site-Directed Spin-Labeling†. *Biochemistry* **1997**, *36*, 13027–13033.
- (49) Oh, K. J.; Altenbach, C.; Collier, R. J.; Hubbell, W. L., Site-directed spin labeling of proteins Applications to diphtheria toxin. In *Bacterial Toxins: Methods and Protocols*; Humana Press, 2000, 145, pp 147–169, DOI: 10.1385/1-59259-052-7:147.
- (50) Drew, D. L., Jr.; Butcher, B.; Sahu, I. D.; Ahammad, T.; Dixit, G.; Lorigan, G. A. Active S2168 and inactive S21IRS pinholin interact differently with the lipid bilayer: A 31P and 2H solid state NMR study. *Biochim. Biophys. Acta Biomembr.* **2020**, 183257–183257.
- (51) Miles, A. J.; Wallace, B. A. Circular dichroism spectroscopy of membrane proteins. *Chem. Soc. Rev.* **2016**, *45*, 4859–4872.
- (52) Altenbach, C.; Flitsch, S. L.; Khorana, H. G.; Hubbell, W. L. Structural studies on transmembrane proteins .2. spin labeling of bacteriorhodopsin mutants at unique cysteines. *Biochemistry* **2002**, *28*, 7806–7812.
- (53) Perozo, E.; Cortes, D. M.; Cuello, L. G. Three-dimensional architecture and gating mechanism of a K+ channel studied by EPR spectroscopy. *Nat. Struct. Biol.* **1998**, *5*, 459–469.
- (54) McHaourab, H. S.; Perozo, E., Determination of protein folds and conformational dynamics using spin-labeling EPR spectroscopy. In *Distance Measurements in Biological Systems by EPR;* Springer: Boston, MA, 2000, 19, pp 185–247.
- (55) Jeschke, G.; Bender, A.; Schweikardt, T.; Panek, G.; Decker, H.; Paulsen, H. Localization of the N-terminal Domain in Light-

- harvesting Chlorophylla/bProtein by EPR Measurements. J. Biol. Chem. 2005, 280, 18623–18630.
- (56) Vásquez, V.; Sotomayor, M.; Cortes, D. M.; Roux, B.; Schulten, K.; Perozo, E. Three-dimensional architecture of membrane-embedded MscS in the closed conformation. *J. Mol. Biol.* **2008**, 378, 55–70.
- (57) McHaourab, H. S.; Lietzow, M. A.; Hideg, K.; Hubbell, W. L. Motion of spin-labeled side chains in T4 lysozyme, correlation with protein structure and dynamics. *Biochemistry* **1996**, *35*, 7692–7704.
- (58) Isas, J. M.; Langen, R.; Haigler, H. T.; Hubbell, W. L. Structure and dynamics of a helical hairpin and loop region in annexin 12: A site-directed spin labeling study. *Biochemistry* **2002**, *41*, 1464–1473.
- (59) Bordignon, E.; Steinhoff, H.-J., Membrane protein structure and dynamics studied by site-directed spin-labeling ESR. In ESR Spectroscopy in Membrane Biophysics; Springer: Boston, MA, 2007, 27, 129–162, DOI: 10.1007/978-0-387-49367-1 5.
- (60) White, G. F.; Schermann, S. M.; Bradley, J.; Roberts, A.; Greene, N. P.; Berks, B. C.; Thomson, A. J. Subunit Organization in the TatA Complex of the Twin Arginine Protein Translocase. *J. Biol. Chem.* **2010**, 285, 2294–2301.
- (61) Tessmer, M. H.; Anderson, D. M.; Buchaklian, A.; Frank, D. W.; Feix, J. B. Cooperative Substrate-Cofactor Interactions and Membrane Localization of the Bacterial Phospholipase A2(PLA2) Enzyme, ExoU. J. Biol. Chem. 2017, 292, 3411–3419.
- (62) Gofman, Y.; Haliloglu, T.; Ben-Tal, N. The transmembrane helix tilt may be determined by the balance between precession entropy and lipid perturbation. *J. Chem. Theory Comput.* **2012**, *8*, 2896–2904.